ISSN (Print) 1226-1750
ISSN (Online) 2233-6656
Journal of Magnetics 28(2), 102-107 (2023) https://doi.org/10.4283/JMAG.2023.28.2.102

Ferrimagnetic and Metallic Properties of (001) $NiCo_2O_4$ Films Fabricated at Various Oxygen Pressures

Jungbae Kim, Yeon Jung Park, and Joonghoe Dho*

Department of Physics, Kyungpook National University, Daegu, Republic of Korea

(Received 21 March 2023, Received in final form 28 April 2023, Accepted 9 May 2023)

Epitaxial (001) $NiCo_2O_4$ films with perpendicular magnetic anisotropy were grown on (001) $MgAl_2O_4$ at various oxygen pressures of 10-200 mTorr using pulsed laser deposition. X-ray diffraction suggested that the lattice constant, crystallinity, and deposition rate displayed distinctive changes around 50 mTorr. The temperature-dependent resistance displayed an insulating behavior in the films grown below 15 mTorr but a metallic one in the films grown above 20 mTorr. Magneto-optical Kerr effect measurement suggested that the $NiCo_2O_4$ films grown above 15 mTorr are ferrimagnetic at room temperature and possess a distinctive perpendicular magnetic anisotropy. The ferrimagnetic-to-paramagnetic transition temperature reached a maximum of ~385 K at 50 mTorr. During the magnetic reversal, the density of small nucleated domains increased with increasing oxygen pressure from 20 to 200 mTorr, and exhibited metallic ferrimagnetism at room temperature. Consequently, the optimal growth condition for magnetic device applications of $NiCo_2O_4$ films is believed to be 50-200 mTorr at 320 ℃.

Keywords: spinel oxide, magnetic film, magnetic anisotropy

1. Introduction

Spinel oxides of AB_2O_4 types (where A and B are transition metal ions) exhibit various physical properties depending on the distribution of 2+ and 3+ metal cations in the octahedral and tetrahedral sites of the cubic spinel structure [1-3]. When a film sample is prepared by the deposition of a bulk target material in a vacuum chamber, it has been reported that the lattice strain of the film can induce changes in the electrical and magnetic properties of the film material [4-11]. In particular, the perpendicular magnetic anisotropy in magnetic films can be induced by lattice distortion, which is accompanied by a change in spin-orbit coupling [12-14]. Many studies on the $NiCo_2O_4$ film with ferrimagnetic and metallic properties have been conducted extensively [16-20]. In the $NiCo_2O_4$, which is a cubic inverse spinel structure, half of the Ni cations and half of the Co cations occupy octahedral sites, while the remaining half of the Co cations occupy tetrahedral sites. However, experimentally synthesized $NiCo_2O_4$ films may have a deviation from the ideal cation distribution and frequently have a mixture of Ni and Co cation distributions. Theoretically, the lattice strain of $NiCo_2O_4$ films can vary magnetic anisotropy because it can induce splitting of the e_g and t_{2g} energy levels related to electron hopping and spin alignment and modifying spin-orbit coupling [21]. Experimental studies have reported that the deposition temperature for synthesizing $NiCo_2O_4$ films with metallic ferrimagnetism is about 250℃-400 ℃. The oxygen partial pressure ranges from tens to hundreds of millitorrs [13, 21-24].

Herein, we investigated the characteristics of (001) $NiCo_2O_4$ films according to oxygen partial pressure. The $NiCo_2O_4$ films were deposited at a fixed temperature of 320 ℃ while varying the oxygen partial pressure from 10 to 200 mTorr. To induce in-plane compressive strain in the $NiCo_2O_4$ film that results in a tetragonal lattice distortion, we deposited it on a (001) $MgAl_2O_4$ single crystal substrate with slightly smaller lattice constants. Additionally, we investigated the perpendicular magnetic anisotropy and magnetic domain structure in (001) $NiCo_2O_4$ films and their structural and transport properties.

2. Experiments

The epitaxial (001) $NiCo_2O_4$ film was fabricated on a

*Corresponding author: Tel: +82-53-950-7354
Fax: +82-53-952-1739, e-mail: jhdho@knu.ac.kr

(001) $MgAl_2O_4$ substrate using pulsed laser deposition. The $NiCo_2O_4$ films were prepared using a polycrystalline target sintered at 1200 °C for 2 hours and a pulsed Nd: YAG laser (wavelength 355 nm, frequency 10 Hz, energy density ~2 J/cm^2) [25, 26]. The deposition temperature and time were fixed at 320 °C and 10 minutes, respectively, while the oxygen pressure was varied from 10 to 200 mTorr. The structural property and surface morphology of the (001) $NiCo_2O_4$ films were characterized by a high-resolution Panalytical X-ray diffraction (XRD) and a Digital Instruments atomic force microscopy (AFM), respectively. The magnetic properties of the $NiCo_2O_4$ films were measured using a magneto-optic Kerr effect (MOKE) setup with an external magnetic field perpendicular to the film plane. A four-point probe method was used to measure the temperature-dependent resistance R(T) of the films with Au electrodes deposited by a direct-current sputtering.

3. Results and Discussion

Figure 1(a) shows the θ-2θ scan XRD pattern of $NiCo_2O_4$ films on (001) $MgAl_2O_4$ deposited at various oxygen pressures ranging from 10 to 200 mTorr. From the XRD measurement, we observed only a (004) peak of the $NiCo_2O_4$ film near the (004) peak of the $MgAl_2O_4$ substrate and no other impurity peaks. This confirms that the $NiCo_2O_4$ films fabricated in this work were epitaxial. Figure 1(b) shows the ω-scan (θ-scan) XRD pattern for the (004) peak of $NiCo_2O_4$. The (004) peaks had a small full width at half maximum (FWHM) values of approximately 0.05°-0.13°. Such small FWHM values imply that our $NiCo_2O_4$ films had good crystalline properties.

The position of the (004) peak of the $NiCo_2O_4$ film shifted slightly toward higher angles as the oxygen pressure increased (Fig. 1(a)). The out-of-plane lattice constant of the $NiCo_2O_4$ film can be estimated from the peak position. Figure 2(a) shows the out-of-plane lattice constant of the $NiCo_2O_4$ film as a function of oxygen pressure. The out-of-plane lattice constant decreased with oxygen pressure, and its variation was relatively small at high oxygen pressures. The out-of-plane lattice constant of the film was slightly larger than that of bulk $NiCo_2O_4$ (a = 8.116 Å), which suggests that the $NiCo_2O_4$ film on (001) $MgAl_2O_4$ experienced a slight expansion along the out-of-plane direction due to compressive in-plane strain caused by the smaller lattice constant of $MgAl_2O_4$ (a = 8.084 Å). In general, a low oxygen pressure during deposition can induce oxygen defects and lattice constant changes in oxide films, making it an important deposition

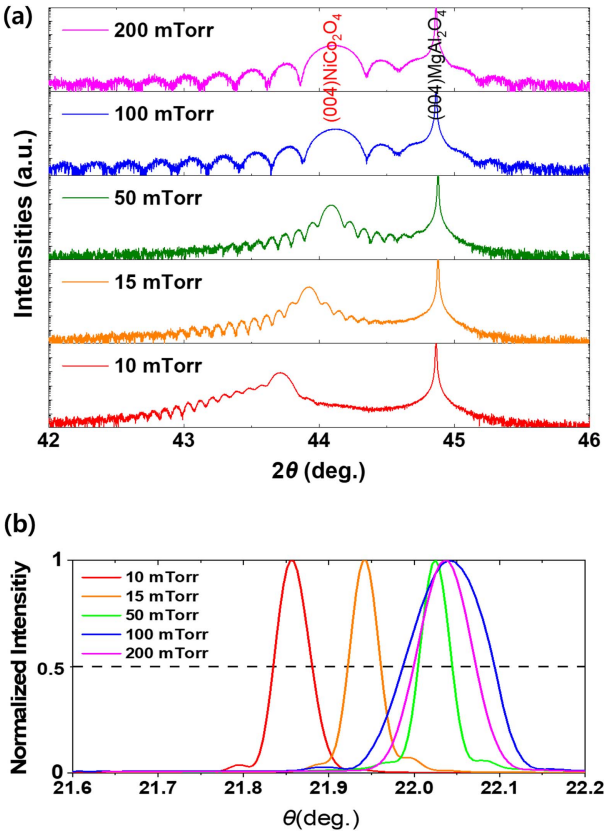

Fig. 1. (Color online) (a) θ-2θ scan and (b) ω-scan X-ray diffraction (XRD) patterns of the (001) $NiCo_2O_4$ films grown on (001) $MgAl_2O_4$ substrate with various oxygen pressure from 10 to 200 mTorr.

parameter. When the deposition temperature is kept constant and the oxygen pressure P_{O2} is reduced, it is thought that the oxygen defect density in the $NiCo_2O_4$ film increases, and the bonding strength between Ni and O ions decreases, leading to an increase in the lattice constant [22].

The interference fringes observed around the (004) peak in Fig. 1(a) confirmed the homogeneous and excellent crystallinity of the film. The period of the interference fringes gives us information on the deposition rate of the film concerning the oxygen partial pressure since the other deposition parameters, such as temperature, laser energy, and deposition time, were fixed during the deposition. The change in the deposition rate of the film with the oxygen partial pressure is caused by collisions between ablated particles and oxygen gas, and it presumably influences the crystallinity of the film related to the FWHM of the ω-scan XRD peak. Figure 2(b) shows the deposition rate and FWHM values of the $NiCo_2O_4$ film as a function of oxygen partial pressure. As the oxygen partial pressure increased, the deposition rate

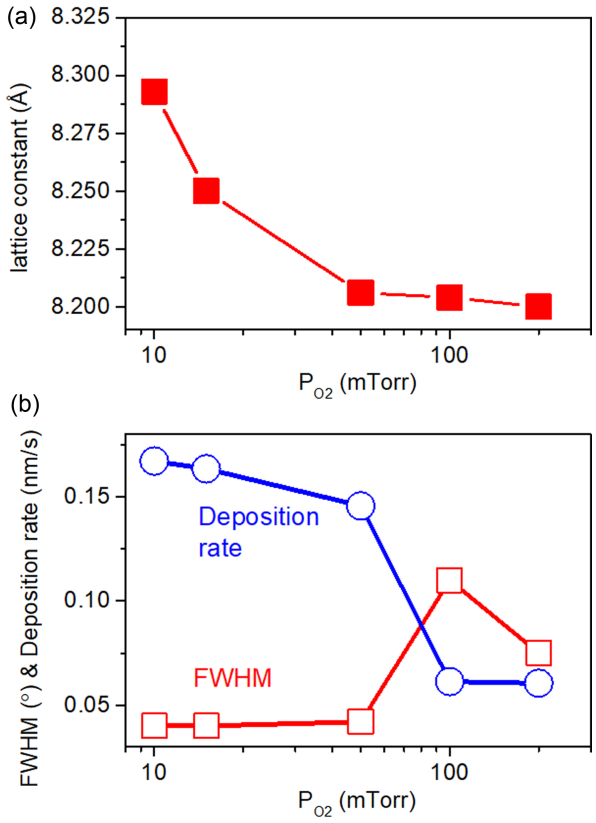

Fig. 2. (Color online) (a) Out-of-plane lattice constants of the (001) $NiCo_2O_4$ films as a function of oxygen pressure (P_{O2}). (b) Full width at half maximum in ω-scan XRD pattern and the deposition rate of $NiCo_2O_4$ film as a function of oxygen pressure.

of the film decreased significantly from 0.14 to 0.06 nm/s in the range 50-100 mTorr. In contrast, the FWHM value of the XRD peak increased significantly from 0.09° to 0.24° in the range 50-100 mTorr. Generally, it is expected that as the deposition rate decreases, the crystallinity will improve, and the FWHM will decrease because the film material can have a longer time to be crystallized. However, it was found that the FWHM of the $NiCo_2O_4$ film increased when the deposition rate decreased. An increase in oxygen partial pressure will induce a decrease in oxygen vacancy and a slight change in the ratio of Ni and Co ions reaching the substrate due to collisions between ablated particles and oxygen gas. The latter probably can cause such an increase in the FWHM of the $NiCo_2O_4$ film with increasing oxygen partial pressure. Energy dispersive X-ray spectroscopy measurement for our films suggested a slight decreasing tendency in the Co/Ni ratio with the oxygen pressure, although a quantitative analysis by profile fitting was unsuccessful because of overlapping Co and Ni peaks.

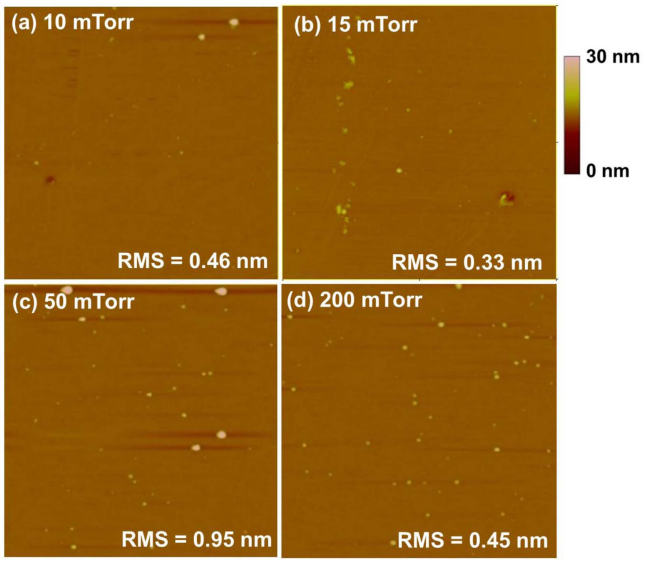

Fig. 3. (Color online) Atomic force microscopy images of the (001) $NiCo_2O_4$ film grown on (001) $MgAl_2O_4$ substrate with various oxygen pressures from 10 to 200 mTorr.

Figure 3 shows AFM images of $NiCo_2O_4$ films deposited at the oxygen partial pressures of 10-200 mTorr. Although small grains, which are frequently observed in pulse laser-deposited films, were seen on the surface of the film, the AFM image showed a relatively flat surface morphology. The root-mean-square (RMS) surface roughness values ranged 0.33-0.95 nm, similar to those in the previously reported 0.6-0.8 nm [17]. Figure 4 shows the temperature dependence of the normalized resistance R(T)/R(T = 290 K) for (001) $NiCo_2O_4$ films fabricated at oxygen pressures of 10-200 mTorr. The as-prepared film at 10

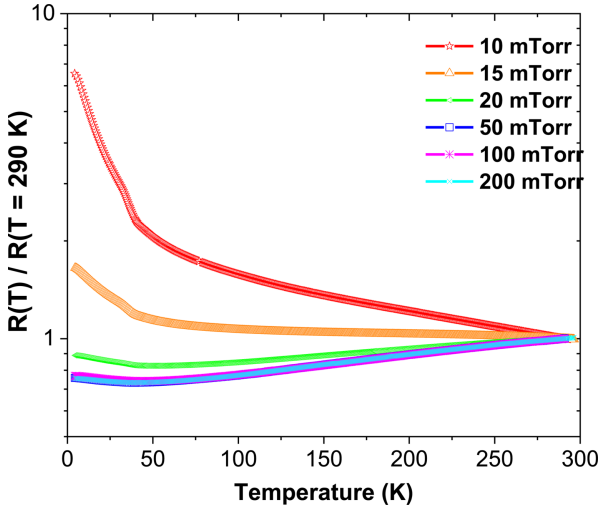

Fig. 4. (Color online) Temperature versus normalized resistance R(T)/R(T = 290 K) for (001) $NiCo_2O_4$ films grown at various oxygen pressures.

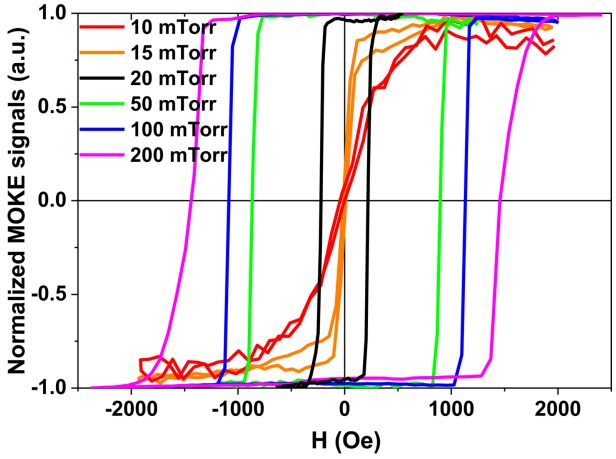

Fig. 5. (Color online) Magnetic field versus normalized magneto–optic Kerr effect signals of (001) $NiCo_2O_4$ films deposited on (001) $MgAl_2O_4$ at room temperature.

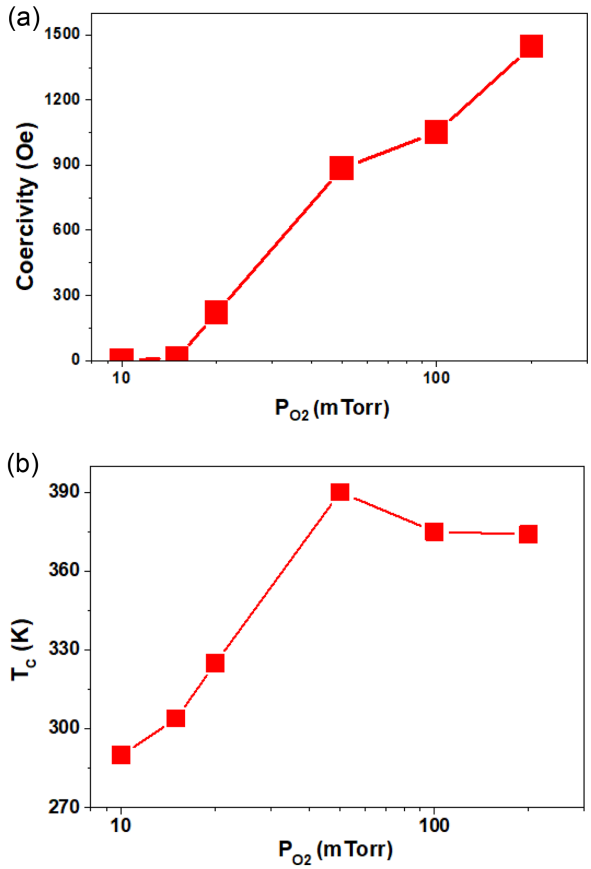

Fig. 6. (Color online) (a) Coercive field (H_C) and (b) Curie temperature (T_C) of the (001) $NiCo_2O_4$ films as a function of oxygen pressure.

mTorr had a resistivity ~3 mΩ·cm at room temperature and showed an increasing tendency as the temperature decreased. Meanwhile, the as-prepared film at 20 mTorr had a resistivity ~0.8 mΩ·cm at room temperature and showed a decreasing tendency as the temperature decreased. That is, the R(T) of the $NiCo_2O_4$ films deposited at 10 and 15 mTorr showed a negative slope near room temperature, indicating semiconductor behavior ($dR/dT < 0$). In contrast, the $NiCo_2O_4$ films deposited above 20 mTorr showed a positive slope, indicating metallic behavior ($dR/dT > 0$).

The (001) $NiCo_2O_4$ film with compressive lattice strain by the (001) $MgAl_2O_4$ substrate is known to exhibit perpendicular magnetic anisotropy [27, 28]. MOKE magnetic hysteresis loops at room temperature were measured by applying a magnetic field perpendicular to the film plane. Figure 5 shows the normalized MOKE magnetic hysteresis loops for (001) $NiCo_2O_4$ films prepared at 10-200 mTorr oxygen partial pressure. The 10 mTorr samples exhibited a superparamagnetic-like magnetic hysteresis loop at room temperature, while the 15 mTorr sample showed a weak ferrimagnetic property with a coercive field of approximately 5 Oe. This is believed to be due to a decrease in the ferrimagnetic transition temperature caused by increased oxygen defects at low oxygen partial pressure. In contrast, when the oxygen partial pressure was increased to 50-200 mTorr, a distinctive perpendicular magnetic anisotropy with a large coercive field of 1000-1500 Oe was observed. The change in oxygen partial pressure is thought to induce changes in oxygen defects, lattice constant, and perpendicular magnetic anisotropy of (001) $NiCo_2O_4$ films [21].

$NiCo_2O_4$ films fabricated above 15 mTorr exhibit ferrimagnetic behavior at room temperature but undergo a ferrimagnetic-to-paramagnetic transition as the temperature increases. The phase transition temperature was investigated by measuring the MOKE signal as a function of temperature. Figure 6 shows the coercivity (H_C) and the critical temperature (T_C) at room temperature as a function of the logarithmic scale of the oxygen partial pressure (P_{O2}). The T_C of the $NiCo_2O_4$ film reached a maximum of 385 K at 50 mTorr. The change in the critical temperature of the $NiCo_2O_4$ film is related to a variation in the spin-spin exchange interaction with oxygen partial pressure. The distribution of cations in $NiCo_2O_4$ can generally be expressed as $Co_x^{2+}Co_{1-x}^{3+}[Co^{3+}Ni_{1-x}^{2+}Ni_x^{3+}]O_4^{2-}$ ($0 < x < 1$) [21, 24]. The ferrimagnetic properties of $NiCo_2O_4$ films can vary depending on the oxygen pressure due to the change in the effective spin value, which is determined by the occupancy of Ni^{2+} ($S = 1$) or Ni^{3+} ($S = 1/2$) at the octahedral sites in the spinel structure [24]. Therefore, low oxygen partial pressure is expected to induce oxygen vacancies and Ni^{2+} ion states, decreasing the ferrimagnetic transition temperature and weakening perpendicular

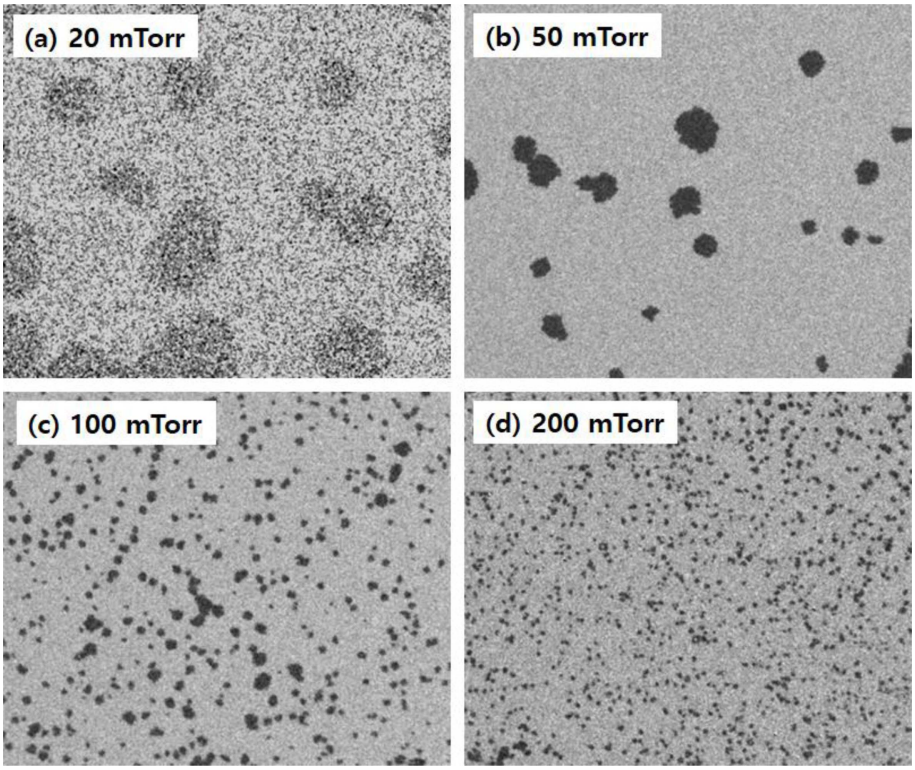

Fig. 7. Magnetic domain structures of (001) $NiCo_2O_4$ films grown at (a) 20 mTorr, (b) 50 mTorr, (c) 100 mTorr, and (d) 200 mTorr. The image size is 810 × 680 μm^2.

magnetic anisotropy at room temperature. On the other hand, a high oxygen partial pressure is expected to decrease oxygen vacancies, increase the ferrimagnetic transition temperature, and strengthen perpendicular magnetic anisotropy at room temperature.

Figure 7 shows the magnetic domain structures of the (001) $NiCo_2O_4$ films at an early stage of magnetic reversal. The magnetic domain structure could be observed in the films grown at 20-200 mTorr, which showed metallic ferrimagnetism and distinctive perpendicular magnetic anisotropy at room temperature. An opposite magnetic field created small magnetic nucleation sites after magnetic saturation. The film grown at 20 mTorr displayed a few nucleated domains with a very weak image contrast. An increase in the oxygen pressure from 20 to 200 mTorr significantly increases the density of the small nucleated domains and image contrast. A connection between the neighboring small domains with an increase in the opposite magnetic field completed the magnetic reversal process. The change in the density of small domains with oxygen pressure is presumably associated with a change in the nucleation sites in the tetragonally distorted (001) $NiCo_2O_4$ films. XRD results suggested that increasing oxygen pressure decreased the tetragonal lattice distortion and the deposition rate. We conjecture that a large lattice distortion and deposition rate induces a large local magnetic fluctuation. Thus, it can make a few nucleation sites even in a small opposite magnetic field. A decrease in the lattice distortion and deposition rate presumably suppresses local magnetic fluctuation and, under a relatively large opposite magnetic field, generates many equivalent nucleation sites in the $NiCo_2O_4$ film.

$NiCo_2O_4$ films fabricated at oxygen pressures of 20-200 mTorr showed strong ferrimagnetism and metallicity at room temperature and distinctive perpendicular magnetic anisotropy. On the other hand, $NiCo_2O_4$ films at an oxygen pressure below 15 mTorr exhibited weak ferrimagnetism and semiconductor behavior, consistent with previous reports [23]. Bitla reported that the mixed ionic state and the coexistence of ferrimagnetism and metallicity in $NiCo_2O_4$ could be explained by the double exchange interaction of Ni^{3+}-O-Ni^{2+} ions [24]. Our study shows that it is possible to fabricate (001) $NiCo_2O_4$ films with potential applications at room temperature by fabricating them at oxygen pressures above 20 mTorr. Additionally, we report that oxygen partial pressure during the film deposition modifies the microscopic domain structure of (001) $NiCo_2O_4$ films during the

magnetic reversal process.

4. Conclusions

Using a pulsed laser deposition, we fabricated epitaxial (001) $NiCo_2O_4$ films on (001) $MgAl_2O_4$ substrates at 320 ℃ while varying the oxygen partial pressure from 10 to 200 mTorr. As the oxygen partial pressure increased, the film's out-of-plane lattice constant and deposition rate decreased distinctively. The $NiCo_2O_4$ films exhibited perpendicular magnetic anisotropy above the oxygen pressure of 15 mTorr and a maximum coercivity of about 1500 Oe at 200 mTorr. Moreover, the ferromagnetic-to-paramagnetic phase transition temperature increased to 385 K as the oxygen partial pressure varied. As the oxygen pressure increased from 20 to 200 mTorr, there was a significant increase in the density of the small nucleated domains during magnetic reversal. This study shows that the oxygen partial pressure is an important deposition parameter that affects the distribution of cations within the material and also its ferromagnetism, metallicity, lattice distortion, and perpendicular magnetic anisotropy. Conclusively, it is thought that $NiCo_2O_4$ films grown at 50-200 mTorr and 320 ℃ can be exploited in various magnetic device applications.

Acknowledgement

This work was supported by The National Research Foundation of Korea (NRF-2021R1F1A1045672). The authors thank Dr. Sang Geul Lee in Korean Basic Science Institute (KBSI) in Daegu for the XRD measurement.

References

[1] J. Lee, S. G. Kwon, J.-G. Park, and T. Hyeon, Nano Lett. **15**, 4337 (2015).
[2] L. Kumar and M. Kar, J. Magn. Magn. Mater. **323**, 2042 (2011).
[3] P. Wang, C. Jin, X. Pang, W. Zheng, G. Gao, D. Wang, D. Zheng, H. Dai, and H. Bai, Appl. Surf. Sci. **493**, 1236 (2019).
[4] C. J. Fennie and K. M. Rabe, Phys. Rev. Lett. **97**, 267602 (2006).
[5] J. H. Lee and K. M. Rabe, Phys. Rev. Lett. **104**, 207204 (2010).
[6] S. P. Bennett, A. T. Wong, A. Glavic, A. Herklotz and C. Urban, et al. Sci. Rep. **6**, 22708 (2016).
[7] S. Mori, C. H. Chen, and S.-W. Cheong, Nature **392**, 473 (1998).
[8] J. Engelmann, V. Grinenko, P. Chekhonin, W. Skrotzki, D. V. Efremov, S. Oswald, K. Iida, R. Hühne, J. Hänisch, M. Hoffmann, F. Kurth, L. Schultz, and B. Holzapfel, Nat. Commun. **4**, 2877 (2013).
[9] H. Guo, S. Dong, P. D. Rack, J. D. Budai, C. Beekman, Z. Gai, W. Siemons, C. M. Gonzalez, R. Timilsina, A. T. Wong, A. Herklotz, P. C. Snijders, E. Dagotto, and T. Z. Ward, Phys. Rev. Lett. **114**, 256801 (2015).
[10] J. H. Ngai, F. J. Walker, and C. H. Ahn, Annu. Rev. Mater. Res. **44**, 1 (2014).
[11] K. H. Ahn, T. Lookman, and A. R. Bishop, Nature **428**, 401 (2004).
[12] B. Tudu and A. Tiwari, Vacuum **146**, 329 (2017).
[13] R. Sbiaa, H. Meng, and S. N. Piramanayagam, Phys. Status Solidi - Rapid Res. Lett. **5**, 413 (2011).
[14] A. B. Shick and O. N. Mr Yasov, Physical Review B **67**, 172407 (2003).
[15] C. F. Windisch Jr., G. J. Exarhos, K. F. Ferris, M. H. Engelhard, and D. C. Stewart, Thin Solid Films **398-399**, 45 (2001).
[16] M. N. Iliev, P. Silwal, B. Loukya, R. Datta, D. H. Kim, N. D. Todorov, N. Pachauri, and A. Gupta, J. Appl. Phys. **114**, 033514 (2013).
[17] W. Guoa, C. Zhena, C. Wua, X. Wub, G. Lic, L. Maa, and D. Houa, Ceram. Int. **44**, 12539 (2018).
[18] C. Wu, W. Guo, C. Zhen, H. Wang, G. Li, L. Ma, and D. Hou, J. Appl. Phys. **126**, 043901 (2019).
[19] H. Sharona, B. Loukya, U. Bhat, R. Sahu, B. Vishal, P. Silwal, A. Gupta, and R. Datta, J. Appl. Phys. **122**, 225301 (2017).
[20] P. Li, C. Xia, J. Li, Z. Zhu, Y. Wen, Q. Zhang, J. Zhang, Y. Peng, H. N. Alshareef, and X. Zhang, ACS Nano **11**, 5011 (2017).
[21] C. Mellinger, J. Waybright, X. Zhang, C. Schmidt, and X. Xu, Phys. Rev. B **101**, 014413 (2020).
[22] K. Zhang, C. Zhen, W. Wei, W. Guo, G. Tang, L. Ma, D. Houa, and X. Wu, RSC Adv. **7**, 36026 (2017).
[23] C. Zhen, X. Zhang, W. Wei, W. Guo, A. Pant, X. Xu, J. Shen, L. Ma, and D. Hou, J. Phys. D: Appl. Phys. **51**, 145308 (2018).
[24] Y. Bitla, Y. Y. Chin, J. C. Lin, C. N. Van, R. Liu, Y. Zhu, H. Liu, Q. Zhan, H. Lin, C. T. Chen, and Y. H. Chu, Sci. Rep. **5**, 15201 (2015).
[25] W. J. Jung and J. Dho. J. Mag. **25**, 126 (2020).
[26] J. Kim and J. Dho, New Physics: Sae Mulli **2**, 167 (2022).
[27] J. Dho and J. Kim, Thin Solid Films **756**, 139361 (2022).
[28] X. Chen, Q. Wu, L. Zhang, Y. Hao, M.-G. Han, Y. Zhu, and X. Hong, Appl. Phys. Lett. **120**, 242401 (2022).